SCIENCE CHINA
Information Sciences

• RESEARCH PAPER •

December 2021, Vol. 64 222401:1–222401:7
https://doi.org/10.1007/s11432-020-3141-3

Flexible plasmonic random laser for wearable humidity sensing

Junhua TONG, Xiaoyu SHI, Yu WANG, Liang HAN & Tianrui ZHAI*

College of Physics and Optoelectronics, Faculty of Science, Beijing University of Technology, Beijing 100124*, China*

Received 28 October 2020/Revised 20 November 2020/Accepted 16 December 2020/Published online 28 September 2021

Abstract Humidity sensing plays an important role in the professional field and our daily life, such as chemical preparation process, environmental monitoring, and food storage. Herein, a wearable humidity sensor is designed based on a flexible plasmonic random laser. The random laser-based humidity sensor is fabricated by transferring an ultrathin light-emitting polymer membrane doped with silver nanoparticles onto the humidity-sensitive PEDOT:PSS film. Under optical pumping, random lasing with low-threshold is achieved, assisted by the strong plasmonic feedback of the silver nanoparticles. The random laser-based humidity sensor exhibits a good linear response with a coefficient of 0.997. Comparing with the emission intensity at initial relative humidity (RH) (34.8%), the peak intensity increases 5.5 times at an RH value of 93.5%. This phenomenon mainly results from the ambient humidity-sensitive relative refractive index difference between polymer membrane and PEDOT:PSS film. The random laser-based humidity sensor is flexible and nontoxic, which can be transplanted easily to achieve wearable laser devices.

Keywords random lasers, humidity sensor, wearable, plasmonic

Citation Tong J H, Shi X Y, Wang Y, et al. Flexible plasmonic random laser for wearable humidity sensing. Sci China Inf Sci, 2021, 64(12): 222401, https://doi.org/10.1007/s11432-020-3141-3

1 Introduction

Random laser is one of the most exciting developments in the past several decades, which can be achieved in various disordered systems by introducing gain. For random lasers, light is localized in an amplifying disordered medium attributed to the multiple scattering process [1–3]. Owing to the superior characteristics including, flexible design, easy preparation, small size and low cost [4–7], random lasers have opened up new opportunities for the fields of speckle-free imaging [8–10], illumination [11], integrated devices [12], medical treatment [13], and sensing [14–18]. In recent years, random lasers have been applied for sensing the pH values [15], biomolecule [16], temperature [17], and bone tissue with nanoscale change [18]. However, random laser-based humidity sensors have been rarely reported.

Humidity is an important indicator to characterize the surrounding environment in technology and daily life. Up to now, some types of optical humidity sensors [19–26] have been explored, such as fiber-based sensors [19–21], FP cavity-based [22], microdisk resonator-based sensors [23, 24], and plasmonic photonic nanostructures-based sensors [25]. Nevertheless, all these sensors need complex preparation and high cost, which hinders their further application. It is necessary to achieve humidity sensors based on random laser for better flexibility and lower cost.

In this study, a plasmonic random laser-based humidity sensor (PRLHS) is designed, fabricated, and demonstrated. The random laser is composed of the ultra-thin gain layer with silver nanoparticles, humidity-sensitive layer and flexible substrate. The random lasing action with low-threshold is achieved owing to the strong plasmonic feedback of the silver nanoparticles. The emission intensity of the proposed structure varies linearly to the ambient humidity, showing good responsivity. Further, we transplant the random laser-based sensor onto different targets, demonstrating excellent humidity sensing performance. The proposed structure can be used as wearable humidity sensors.

* Corresponding author (email: trzhai@bjut.edu.cn)

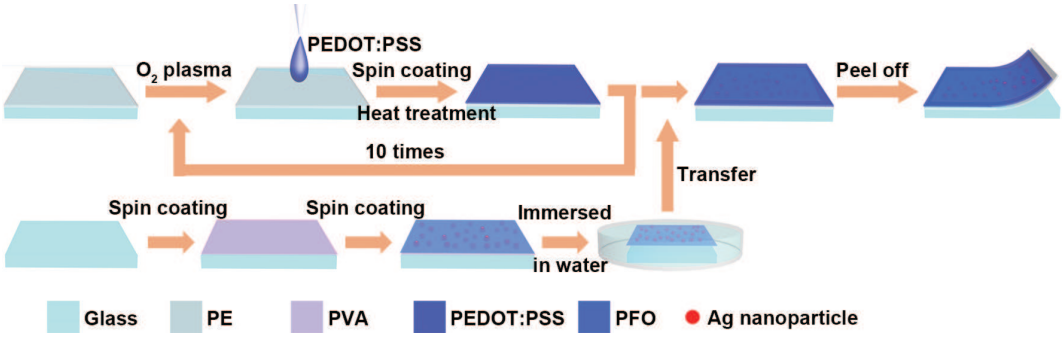

Figure 1 (Color online) Schematic illustration of the fabrication process of the PRLHS.

2 Experiments

2.1 Fabrication of PRLHS

A plastic cling wrap film with a thickness of 0.25 mm (Miaojie PE film) is cut into pieces with 22 mm in length and 22 mm in width. As shown in Figure 1, one piece of PE film is chosen to attach tightly and flatly on the glass substrate (20 mm × 20 mm × 1 mm). To improve its hydrophilicity, the surface of the PE film is treated with O_2 plasma for 90 s at a power of 25 W (Plasma Cleaner: PDC-32G). Subsequently, the aqueous PEDOT:PSS dispersion (Innochem: Clevios pH 1000) is spin-coated on the plasma-treated PE film at a speed of 2000 rpm for 30 s, and then dried on the heating plate at 60°C for 2 min. After drying, the O_2 plasma is applied for 30 s at the power of 25 W on the PEDOT:PSS surface for spin-coating the second PEDOT:PSS layer as described above. Note that the O_2 plasma is used to increase the hydrophilic groups on the surface of PEDOT:PSS film. The interface quality of the multilayer structure can be improved significantly during the multiple spin-coating process owing to the enhancement of the hydrophilicity of PEDOT:PSS. Repeatedly, the tenth PEDOT:PSS layer is spin-coated. The multilayer structure of PEDOT:PSS is designed for reducing the mechanical damage during working [27]. Then, the PE/PEDOT:PSS structure is dried on the heating plate at 60° for 30 min, forming a humidity-sensitive PE/PEDOT:PSS film.

The active layer is a typical blue light-emitting polymer (PFO) membrane doped with Ag nanoparticles, which is obtained based on our fabrication method previously reported [28]. As shown in Figure 1, PVA (Polyvinylalcohol, Celanese Chemicals) aqueous solution (40 mg/mL) is spin-coated on a glass substrate (20 mm × 20 mm × 1 mm) at a speed of 3000 rpm for 30 s, forming a water soluble layer. Subsequently, a xylen solution of PFO light-emitting polymer (12.5 mg/mL) and Ag nanoparticles (0.05 mg/mL) is spin-coated on the PVA layer at a speed of 1500 rpm for 30 s, forming a gain layer with the thickness of 200 nm. Next, the PVA layer is dissolved by immersing the prepared structure into deionized water, achieving a free-standing PFO membrane doped with Ag nanoparticles.

The free-standing active membrane is then transferred onto the PE/PEDOT:PSS composite film on the glass substrate. The active membrane is sticking tightly and smoothly to the PEDOT:PSS film after drying naturally because of surface tension. Finally, the PE/PEDOT:PSS/PFO+Ag NPs PRLHS is achieved by peeling the plastic cling wrap film off the glass substrate, as shown in Figure 1.

2.2 Characterization and measurement

SEM images are taken with a field-emission scanning electron microscope (FE-SEM: Hitachi S-4800). The relative humidity (RH) is controlled using a humidifier and measured in a home-made closed vessel (P = 101.3 KPa, T = 23°) using a digital temperature/humidity meter (PM6508). Eight values of RH ranges of 34.8%, 43.1%, 51.6%, 59.7%, 67.5%, 76.2%, 85% and 93.5% are generated by controlling the working time of the humidifier for 0, 5, 20, 40, 60, 90, 120, 150 s, respectively. A frequency-doubled pulse laser (400 nm, 200 fs, 1 kHz) is used as a pump source and a spectrometer (Maya 2000 Pro, Ocean Optics) is used to collect the emission spectra.

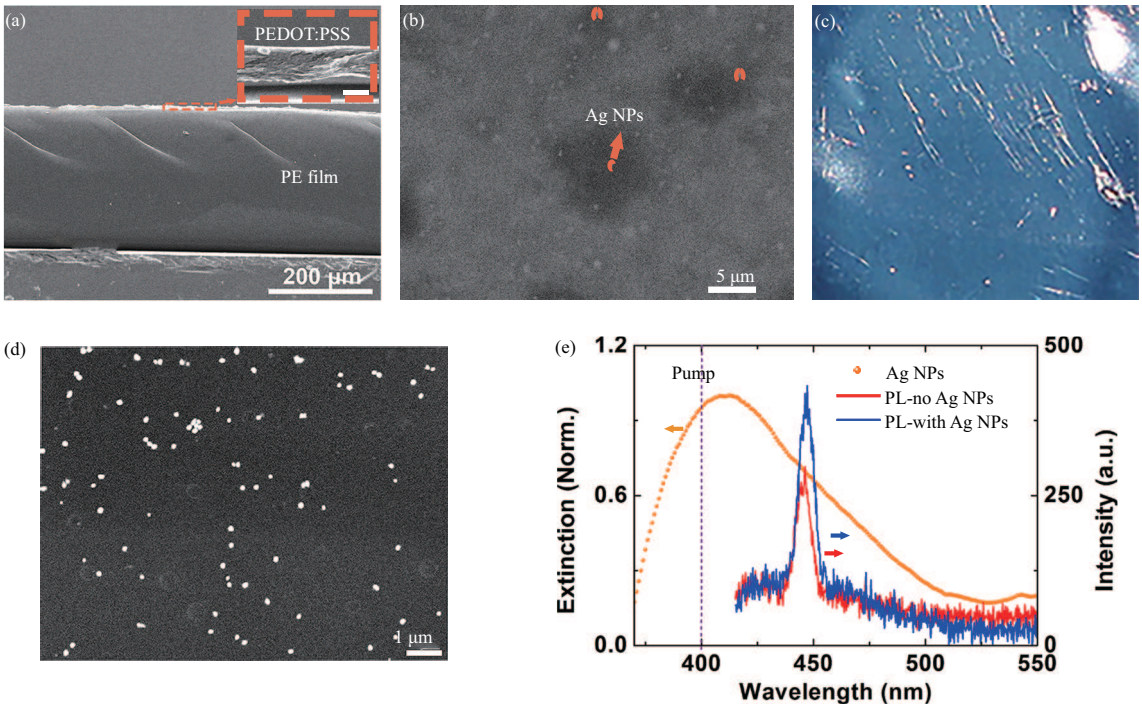

Figure 2 (Color online) (a) Cross section SEM image of the PE/PEDOT:PSS composite film. Inset: PEDOT:PSS layer at high magnification, scalar bar: 2 μm. (b) Top-view SEM image of the PRLHS. The orange circles indicate the Ag NPs. (c) Photograph of the PRLHS. (d) SEM image of Ag NPs. (e) Extinction spectrum of Ag NPs, PL spectra of PRLHS with/without Ag NPs. The violet dash line denotes the wavelength of the pump source (400 nm, 200 fs, 1 kHz).

3 Results and discussion

Figure 2(a) shows the cross section of the PE/PEDOT:PSS composite film, indicating the thickness of multilayer PEDOT:PSS is about 3 μm. The active layer is smoothly attached onto the PEDOT:PSS film, and the Ag NPs are distributed randomly in the PFO membrane, which can be seen in Figures 2(b) and (c). The Ag NPs have a uniform size with a diameter around 100 nm, as shown in Figure 2(d). Figure 2(e) shows the extinction spectrum of Ag NPs and the fluorescence spectra of PFO with/without Ag NPs. The plasmonic resonance peak of Ag NPs overlaps with both the fluorescence peak of the PFO and the pump wavelength, which can provide enhancement of excitation and emission simultaneously [29], as shown in Figure 2(e).

Random lasing action is demonstrated in Figure 3. Figure 3(a) shows the emission spectra of PRLHS at different pump energy densities. With the increase of the pump energy density, the emission spectrum is changing from the typical fluorescent characteristics to random lasing performances. Figure 3(b) shows the curves of the emission intensity and the full width at half maximum (FWHM) at the wavelength of 448 nm and the pump energy density. The FWHM decreases from 16 nm to around 4 nm. The threshold behavior is observed obviously, showing the threshold around 13.1 μJ/cm^2. The low threshold is mainly attributed to the plasmonic enhancement of Ag nanoparticles and the waveguide effect of the active layer. On basis of the low threshold and spectral behavior, we can conclude the onset of random lasing action [30, 31].

The influence of the RH on lasing performances of PRLHS is studied by controlling the RH values. The corresponding emission spectra are collected, as shown in Figure 4(a). In the experiment, the pump power is fixed during the spectroscopic measurement. For the proposed incoherent random laser, the emission is very stable. At low RH values, the random lasing spectrum is observed with weak peak intensity. As the RH value increases, the emission peak intensity increases significantly. Figure 4(b) shows the corresponding emission peak intensities of PRLHS varying with the RH values, which exhibit a linear relationship with a coefficient (R^2) of 0.997. Besides, the emission intensity changes within several seconds after absorbing water vapor owing to the exceptional humidity sensitivity of the PEDOT:PSS layer. Whereas, the emission peak intensity in the sample without PEDOT:PSS layer is almost unchanged with the RH value changes, as shown in Figure 4(b). These results indicate the humidity sensing effect in

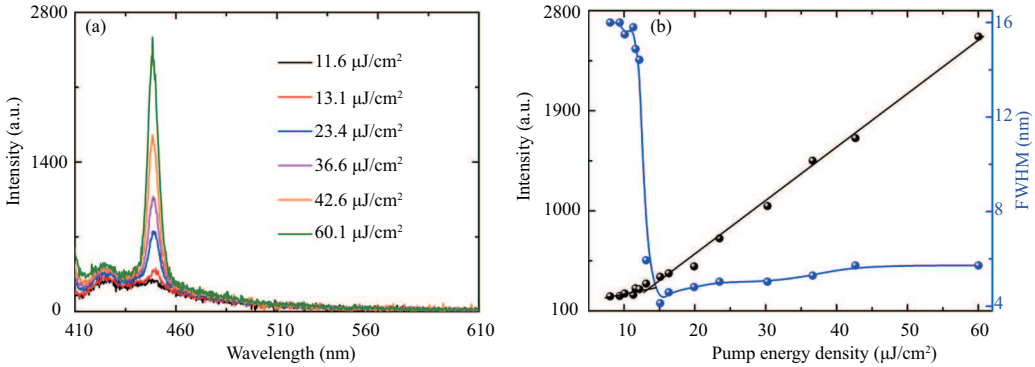

Figure 3 (Color online) Random lasing actions in the random laser-based humidity sensor at original RH (34.8%). (a) Emission spectra at different pump energy densities. (b) Emission intensity (black spheres) and the linewidth (blue spheres) as a function of the pump energy density.

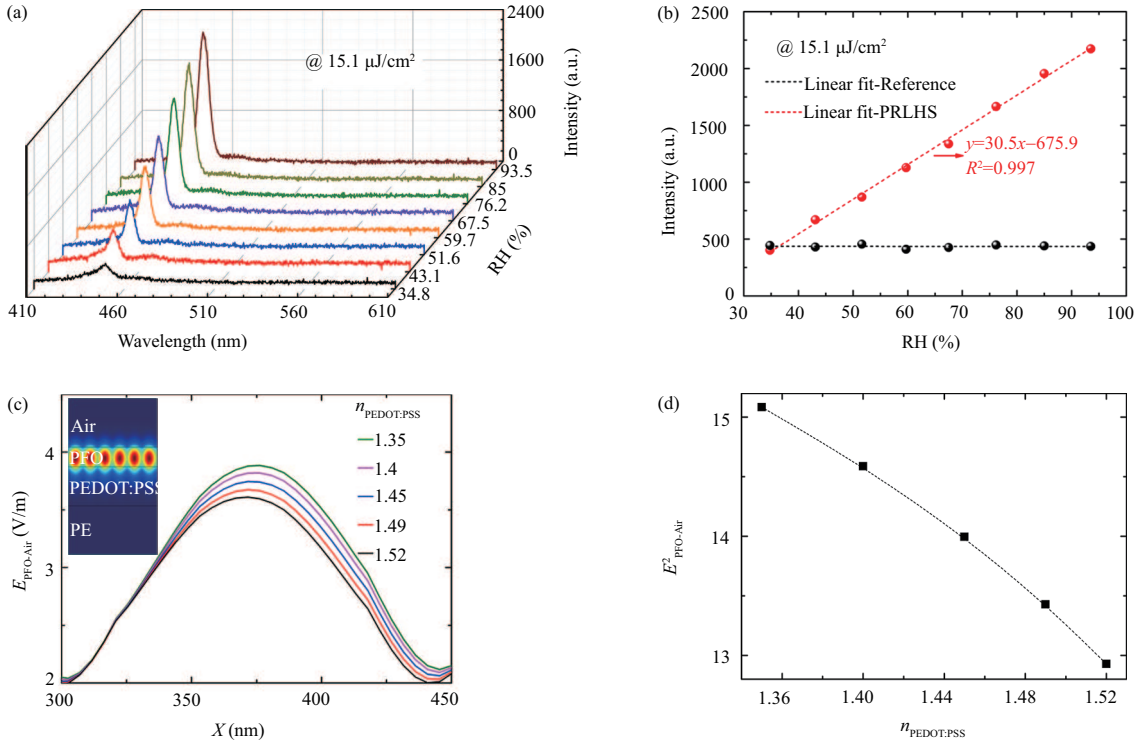

Figure 4 (Color online) (a) The emission spectra of the PRLHS at different humidifies under the pump energy density of 15.1 μJ/cm^2 ($n_{\mathrm{PEDOT:PSS}}$ = 1.49). (b) Peak intensities of emission spectra in PRLHS and reference substance with/without PEDOT:PSS layer vary with the RH values. The spheres are the experimental data, and the dashed line is the corresponding linearly fitted curve. (c) Electric field distributions at the interface of PFO layer and air layer. Inset: the electric field distribution of the corresponding PE/PEDOT:PSS/PFO structure at 448 nm. (d) The electric field intensity ($E^2_{\mathrm{PFO\text{-}Air}}$) at the interface of PFO layer and air layer varies with the refractive index of PEDOT:PSS layer ($n_{\mathrm{PEDOT:PSS}}$ = 1.35 − 1.49).

PRLHS resulted from the PEDOT:PSS layer [27]. In our experiment, temperature disturbance induced by pumping and evaporating process may affect the sensor intensity. However, the sample is pumped by a femtosecond pulse laser for a short time. Besides, water vapor evaporates relatively slowly owing to the sample in the hermetic room. The temperature changes in a small range, contributing to slight changes of the output light intensity in the composite film humidity sensor [32]. Therefore, the temperature disturbance can be ignored in our experiment. However, for practical applications, temperature calibration should be included. One of the possible temperature compensation methods is to simultaneously measure RH concentration and temperature with cascaded sensors. One sensor is used to sense the temperature and humidity simultaneously. The other same sensor is encapsulated to sense the temperature only.

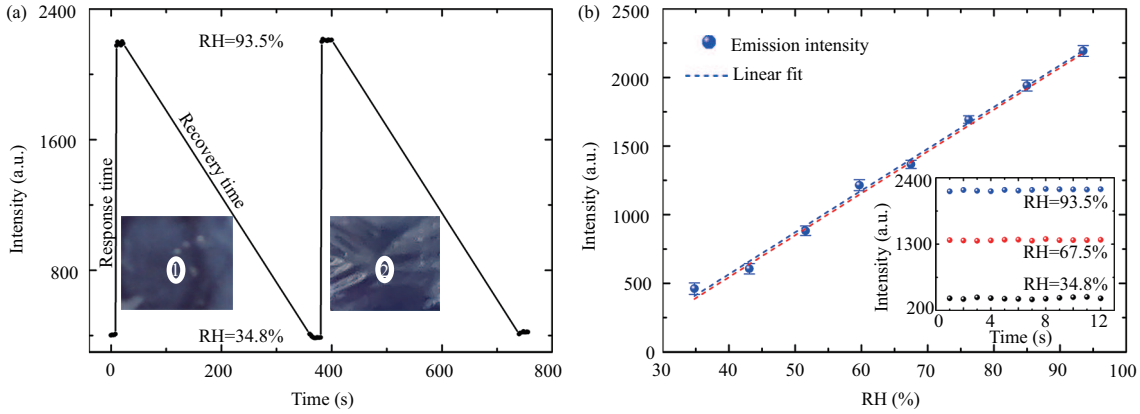

Figure 5 (Color online) The repeatability of PRLHS after several wetting and drying cycles. (a) Reversibility of the sample between RH 67.5% and 76.2% (P = 101.3 KPa, T = 23°C). Inset: Images of the sample before ① and after ② wetting and drying cycles. (b) Peak intensities of emission spectra in the sample as a function of RH values. The blue dots denote the experimental data. The blue dashed line corresponds to its linear relationship. Inset: The time response of the sample at three RH values for calculating the σ_{D} in the experiment.

The sensitivity (S) of PRLHS is defined as

$$S = \frac{\Delta I/I_0}{\Delta \mathrm{RH}}, \tag{1}$$

where I_0 is the emission peak intensity at the original humidity, ΔI is the change in emission peak intensity and ΔRH is the corresponding variety in RH. The sensitivity is calculated to be 7.5/RH. Further, the limit of detection (LOD) of our proposed humidity sensor is calculated according to

$$\mathrm{LOD} = 3.3\sigma_D/b, \tag{2}$$

where b is the slope of the peak intensity versus RH curve, as shown in Figure 4(b). σ_D is the standard deviation of the emission intensity [33, 34]. According to the inset image in Figure 5(b), σ_D can be calculated as 13.05 a.u. Therefore, the LOD is calculated as 1.41% RH in our experiment.

The repeatability of the PRLHS is a crucial parameter for the humidity sensor. The reversibility of the sample between RH 34.8% and 93.5% is presented in Figure 5(a), indicating the good reversibility with a short response time (few seconds). However, the recovery time is long for few minutes because the water vapor evaporates relatively slowly in our experiment. The inset images in Figure 5(a) show the images of the sample before ① and after ② wetting and drying cycles. There are some wrinkles on the sample after wetting and drying cycles, which have little influence on the lasing performance. Figure 5(b) shows the emission peak intensities varying with the RH values in the sample after wetting and drying cycles. Obviously, it follows a linear relationship (blue dashed line), which overlaps with the linearly fitted curve of the original sample in Figure 4(b).

In the process of water absorption, the effective refractive index of PEDOT:PSS layer is decreasing, which leads to the higher refractive index difference between the humidity layer and active layer. The higher refractive index difference contributes to the stronger optical feedback in the active cavity and the lower lasing threshold. Therefore, the emission peak intensity in PRLHS becomes stronger as the refractive index of PEDOT:PSS layer decreases. Furthermore, the electric field pattern of PE/PEDOT:PSS/PFO structure is simulated using the finite element method in COMSOL, as shown in the inset of Figure 4(c). Here, the non-periodic boundary is added to avoid boundary conditions interfering with evanescent fields. The refractive index of the PFO is 1.85. The electric field distribution curves at the interface of PFO layer and air layer at different refractive indexes of PEDOT:PSS layer are extracted, indicating that the stronger electric field intensity obtained in PEDOT:PSS layer with lower refractive index, as shown in Figure 4(d). Besides, in the water volatilization process, the emission peak intensity decreases to the original state. All the results indicate the emission intensity of random lasing in PRLHS is sensitive to the RH, which provides a new way for humidity sensing.

In recent years, wearable device has attracted much attention arising from their potential application in healthy and motion data monitoring [35, 36]. The proposed PRLHS is flexible and nontoxic, which can be applied as a humidity sensor and wearable laser device. We transplant the PRLHS onto an apple slice after one hour and 48 hours standing, as shown in Figures 6(a) and (b).

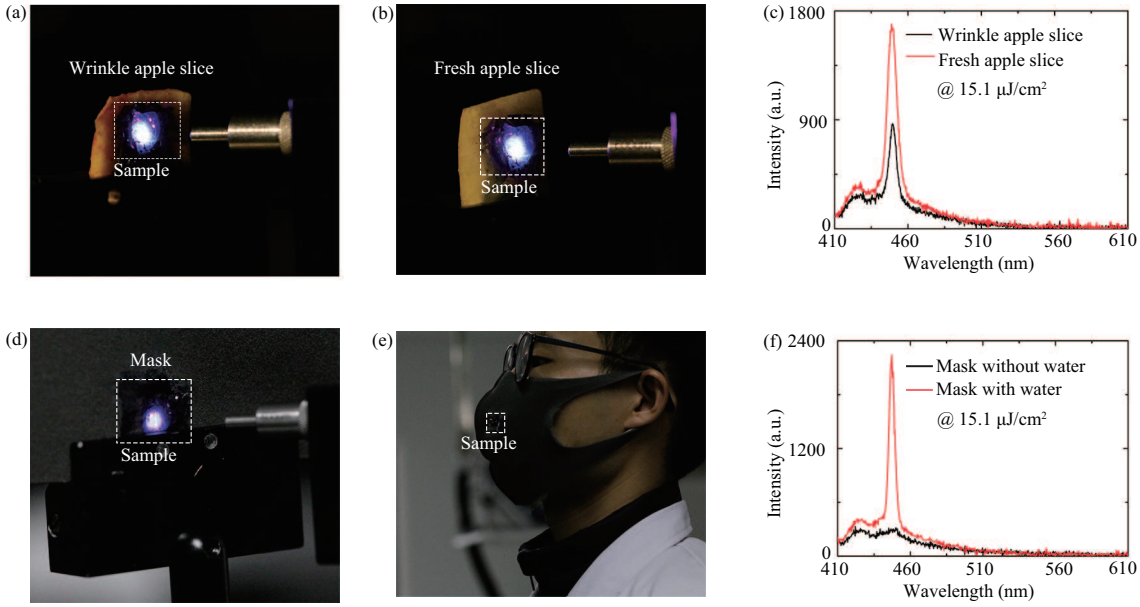

Figure 6 (Color online) The flexibility and wearability of the proposed PRLHS. Water content sensor attached on (a) the wrinkle apple slice and (b) fresh apple slice. (c) The corresponding emission spectra of PRLHS on wrinkle/fresh apple slices. (d) PRLHS attached on the mask. (e) The wearable showing. (f) The emission spectra of PRLHS before/after water spraying on the mask. In our experiment, the exciting light is perpendicular to the surface of the sample. The intensity of the laser beam is controlled by a variable optical attenuator. The reflected light is collected by the spectrometer. The detector is fixed at an angle of about 45° to the sample surface.

The corresponding emission spectra of the PRLHS are shown in Figure 6(c). At the same pump energy density, the emission intensity of the PRLHS on the apple slice with one hour standing is twice as strong as that on the apple slice after 48 hours standing, indicating the apple slice with one hour standing is wetter. Therefore, our proposed PRLHS can be used as sensors for measuring water content in fruits. A wearable humidity sensor is achieved by transplanting the PRLHS onto a washable mask, as shown in Figures 6(d) and (e). In addition, we have studied the influence of water on the emission intensity of the proposed wearable PRLHS, as shown in Figure 6(f). The experiment result shows the emission intensity is dramatically enhanced after spraying the water vapor on the mask. It can be attributed to a lower effective refractive index of PEDOT:PSS layer caused by a higher value of the ambient RH. This property can be used for monitoring and evaluating the amount of perspiration.

4 Conclusion

In summary, a PRLHS with the structure of PE/PEDOT:PSS/PFO+Ag nanoparticles is achieved. The PEDOT:PSS film and Ag NPs doped PFO membrane act as the humidity-sensitive layer and the laser layer, respectively. Assisted by the strong plasmonic feedback of the silver nanoparticles, low threshold random lasing is observed under optical pumping. The emission intensity of PRLHS is increased effectively by increasing the RH value, which is resulted from the decrease of the refractive index of PEDOT:PSS layer during the water absorption process. Finally, we have transplanted the PRLHS onto an apple slice and a mask, obtaining the food freshness sensors and the wearable laser sensor. We believe that our proposed PRLHS may promote the practical application of random lasing in sensors and wearable laser devices.

Acknowledgements This work was supported by National Natural Science Foundation of China (Grant Nos. 61822501, 12004017) and Beijing Natural Science Foundation (Grant Nos. Z180015, 1204028).

References

1 Lawandy N M, Balachandran R M, Gomes A S L, et al. Laser action in strongly scattering media. Nature, 1994, 368: 436–438
2 Cao H, Zhao Y G, Ho S T, et al. Random laser action in semiconductor powder. Phys Rev Lett, 1999, 82: 2278–2281
3 Wiersma D S. The physics and applications of random lasers. Nat Phys, 2008, 4: 359–367
4 Luan F, Gu B, Gomes A S L, et al. Lasing in nanocomposite random media. Nano Today, 2015, 10: 168–192
5 Wiersma D. The smallest random laser. Nature, 2000, 406: 133–135

6 Li X, Liu H, Xu X, et al. Lotus-leaf-inspired flexible and tunable random laser. ACS Appl Mater Interfaces, 2020, 12: 10050–10057
7 Xia J, Xie K, Ma J, et al. The transition from incoherent to coherent random laser in defect waveguide based on organic/inorganic hybrid laser dye. Nanophotonics, 2018, 7: 1341–1350
8 Zhang X, Yan S, Tong J, et al. Perovskite random lasers on fiber facet. Nanophotonics, 2020, 9: 935–941
9 Bian Y, Shi X, Hu M, et al. A ring-shaped random laser in momentum space. Nanoscale, 2020, 12: 3166–3173
10 Xie Z, Xie K, Hu T, et al. Multi-wavelength coherent random laser in bio-microfibers. Opt Express, 2020, 28: 5179–5188
11 Redding B, Choma M A, Cao H. Speckle-free laser imaging using random laser illumination. Nat Photon, 2012, 6: 355–359
12 Zhai T, Niu L, Cao F, et al. A RGB random laser on an optical fiber facet. RSC Adv, 2017, 7: 45852–45855
13 Hsu Y T, Lin Y Y, Chen Y Z, et al. 3D printed random lasers. Adv Mater Technol, 2020, 5: 1900742
14 Gaio M, Caixeiro S, Marelli B, et al. Gain-based mechanism for pH sensing based on random lasing. Phys Rev Appl, 2017, 7: 034005
15 Ignesti E, Tommasi F, Fini L, et al. A new class of optical sensors: a random laser based device. Sci Rep, 2016, 6: 35225
16 Shi X, Ge K, Tong J H, et al. Low-cost biosensors based on a plasmonic random laser on fiber facet. Opt Express, 2020, 28: 12233–12242
17 Wang Z N, Rao Y J, Wu H, et al. Long-distance fiber-optic point-sensing systems based on random fiber lasers. Opt Express, 2012, 20: 17695–17700
18 Song Q, Xu Z, Choi S H, et al. Detection of nanoscale structural changes in bone using random lasers. Biomed Opt Express, 2010, 1: 1401–1407
19 Zhang Z F, Zhang Y. Humidity sensor based on optical fiber attached with hydrogel spheres. Opt Laser Tech, 2015, 74: 16–19
20 Krämmer S, Laye F, Friedrich F, et al. Electrospun polymer fiber lasers for applications in vapor sensing. Adv Opt Mater, 2017, 5: 1700248
21 Zhao Y, Tong R, Chen M Q, et al. Relative humidity sensor based on hollow core fiber filled with GQDs-PVA. Sens Actuat B-Chem, 2019, 284: 96–102
22 Shi J, Xu D, Xu W, et al. Humidity sensor based on fabry-perot interferometer and intracavity sensing of fiber laser. J Lightwave Technol, 2017, 35: 4789–4795
23 Eryürek M, Tasdemir Z, Karadag Y, et al. Integrated humidity sensor based on SU-8 polymer microdisk microresonator. Sens Actuat B-Chem, 2017, 242: 1115–1120
24 Labrador-Páez L, Soler-Carracedo K, Hernández-Rodríguez M, et al. Liquid whispering-gallery-mode resonator as a humidity sensor. Opt Express, 2017, 25: 1165–1172
25 Wang Y, Liu F, Zhang X. Flexible transfer of plasmonic photonic structures onto fiber tips for sensor applications in liquids. Nanoscale, 2018, 10: 16193–16200
26 Hu M, Bian Y, Shen H, et al. A humidity-tailored film random laser. Org Electron, 2020, 86: 105923
27 Wang G, Xia H, Sun X C, et al. Actuator and generator based on moisture-responsive PEDOT: PSS/PVDF composite film. Sens Actuat B-Chem, 2018, 255: 1415–1421
28 Zhai T, Xu Z, Wu X, et al. Ultra-thin plasmonic random lasers. Opt Express, 2016, 24: 437–442
29 Liu S Y, Huang L, Li J F, et al. Simultaneous excitation and emission enhancement of fluorescence assisted by double plasmon modes of gold nanorods. J Phys Chem C, 2013, 117: 10636–10642
30 Tong J, Li S, Chen C, et al. Flexible random laser using silver nanoflowers. Polymers, 2019, 11: 619
31 Liu Y, Yang W, Xiao S, et al. Surface-emitting perovskite random lasers for speckle-free imaging. ACS Nano, 2019, 13: 10653–10661
32 Wang Y, Shen C, Lou W, et al. Fiber optic humidity sensor based on the graphene oxide/PVA composite film. Opt Commun, 2016, 372: 229–234
33 Sunilkumar A, Manjunatha S, Chethan B, et al. Polypyrrole-tantalum disulfide composite: an efficient material for fabrication of room temperature operable humidity sensor. Sens Actuat A-Phys, 2019, 298: 111593
34 Caucheteur C, Guo T, Liu F, et al. Ultrasensitive plasmonic sensing in air using optical fibre spectral combs. Nat Commun, 2016, 7: 13371
35 Ma B W, Zou W W. Demonstration of a distributed feedback laser diode working as a graded-potential-signaling photonic neuron and its application to neuromorphic information processing. Sci China Inf Sci, 2020, 63: 160408
36 Wang G, Zhang Y, Yang H, et al. Fast-response humidity sensor based on laser printing for respiration monitoring. RSC Adv, 2020, 10: 8910–8916